On the Existence of Different Zeolite-Associated Topological Redox Isomers. Electrochemistry of the Y Zeolite-Associated Mn(Salen)N_3 Complex

Antonio Doménech*

Departamento de Química Analítica, Universidad de Valencia, Dr. Moliner 50, Burjassot (Valencia) 46100, Spain

Pilar Formentín, Hermenegildo García, and María J. Sabater

Instituto de Tecnología Química UPV-CSIC, Universidad Politécnica de Valencia, Aptdo. 22012, 46071 Valencia, Spain

Received: April 9, 2001; In Final Form: July 20, 2001

The electrochemical properties of Y zeolite-associated Mn^{III}(salen)N_3 (salen = *trans*-(*R*,*R*)-1,2-bis(salicyldeneamino)cyclohexane) has been investigated using polymer film electrodes immersed into neutral aqueous solutions. Zeolite Y-associated Mn(III)−salen complexes are reduced in one-electron reversible process at −0.25 V versus SCE. The electrochemical response is discussed in terms of the existence of two topological redox isomers: a weakly boundary-associated Mn(salen) complex, whose electrochemical response corresponds to a reversible one-electron transfer controlled by diffusion of the positive ions of the supporting electrolyte through the zeolite surface windows and channels, and a strongly boundary-associated Mn(salen) complex for which the electrochemical response parallels that of reagents attached to the electrode surface. Kinetic and thermochemical data for such processes are obtained from the temperature dependence of electrochemical parameters.

1. Introduction

Immobilization of metal complexes inside the rigid matrix of microporous solids has been researched intensively in recent years because of the catalytic properties of this kind of system. Incorporation of complexes on to an inorganic support makes it possible to perform catalytic reactions combining the advantages of homogeneous and heterogeneous catalytic systems.[1,2] This is the case of the chiral Mn^{III}(salen) complex (salen = *trans*-(*R*,*R*)-1,2-bis(salicyldeneamino)cyclohexane), which is an efficient epoxidation catalyst in both homogeneous and heterogeneous phases.[3−6]

Zeolites are a large family of crystalline aluminosilicates whose structure defines channels and cavities of molecular dimensions in which molecules can be trapped. Site isolation and steric confinement, in combination with the ability for cationic mobility, contribute to the development of sterically and ionically selective sensors.

Accordingly, the electrochemistry of metal complexes encapsulated into zeolites has been widely studied.[7] The electrochemistry of cobalt, iron, and manganese salen complexes encapsulated into zeolites has been investigated in nonaqueous media using graphite electrodes (carbon paste and pressed powder composite electrodes)[8−11] and stirred dispersions at a large surface area electrode.[12]

The interpretation of data, however, has become controversial.[13,14] Electrochemical processes occurring at zeolite-modified electrodes have been described as electron-transfer processes occurring outside of the zeolite after ion exchange of electroactive species with electrolyte cations,[15−18] or involving species located in the supercages of the outer cavities or subsurface zones.[11,19−21] The surface mediated electron-transfer mechanism consists on the propagation of electrons through the neighboring zeolite supercages.[22−24] A problem that arises from the consideration of the different electrochemical mechanisms that have been proposed is whether the same complex can exhibit an specific electrochemical behavior, depending on its location on the zeolite particle.[7,25]

Following Turro and García-Garibay[26] and Bessel and Rolison,[25] different topological redox isomers can be responsible for the electrochemistry observed in zeolite-associated species. Thus, the redox-active molecules can be (i) outside the zeolite, with no bonding or sorptive association, (ii) bound to the boundary (or external surface) of the zeolite, (iii) adsorbed into the voids of the zeolite but able to sample the global pore lattice topology, or (iv) size-included in the interior of a supercage or a channel intersection of the zeolite. Although this idea has been pursued, no evidence for a specific electrochemical behavior of topological isomers has been obtained so far.

The current work reports an study of the electrochemistry of Mn(salen)N_3−zeolite Y systems attached to polymer film electrodes (PFEs) immersed into not only nonaqueous solvents, as so far reported, but also into aqueous solutions. This study attempts to establish a valid scheme to prove the existence of different electroactive topological redox isomers.

Since additional families of topological redox isomers having different coordination environments around the electroactive

* Corresponding author. E-mail: antonio.domenech@uv.es.

10.1021/jp011315j CCC: $22.00
Published on Web 01/17/2002

SCHEME 1: Schematic for the Formation of Y Zeolite-Encapsulated Mn(Salen)N_3 Complex

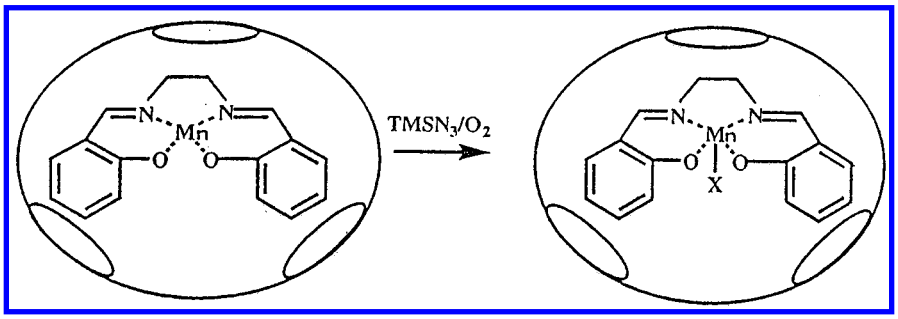

centers can exist as a result of a distribution of interactions with the zeolite framework, a complex possessing identical coordination environment in solution and in the zeolite sites is required for properly distinguishing between the electrochemical behavior of such species in solution and associated to the zeolite boundary. Accordingly, the electrochemical response of the parent Mn(salen)N_3 and Mn(salen)Cl complexes in solution is compared with those of the zeolite-associated Mn(salen)N_3 complex. To discard interfering surphace phenomena, the electrochemistry of solid Mn(salen)X (X = Cl, N_3) complexes attached to the electrode surface as dry powders is also studied. The electrochemical response of the zeolite-associated Mn(salen)N_3 complex has been studied by linear scan voltammetry (LSV), cyclic voltammetry (CV), and differential pulse voltammetry (DPV). The electrochemical behavior is discussed in terms of the existence of two topological redox isomers: a weakly boundary-associated Mn(salen) complex and a strongly boundary-associated Mn(salen) complex.

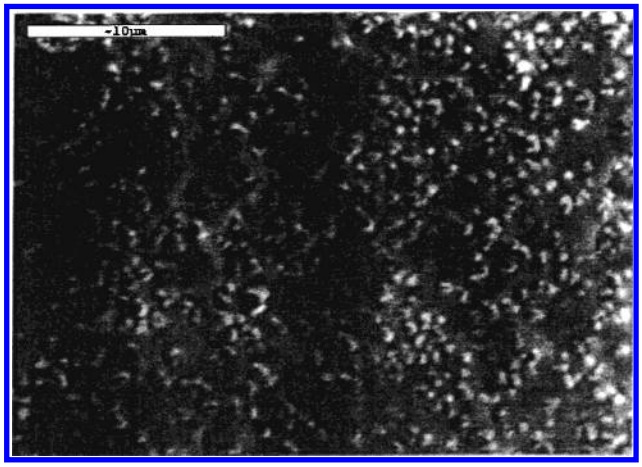

Figure 1. SEM image of a zeolite-modified Paraloid B72 film electrode.

2. Experimental Section

Synthesis of $Mn^{III}(salen)^+$ inside the pores of zeolite Y was carried out as previously reported[6] by condensation of *trans*-(*R*,*R*)-1,2-diamino-cyclohexane and salicylaldehyde around the Mn^{2+} ions resident in the supercages of the Mn^{2+}-preexchanged zeolite Y (0.48% Mn^{2+}, measured by atomic absorption spectroscopy; approximately 1 Mn^{2+} every 5 supercages), followed by treatment with molecular oxygen.

The Y zeolite-encapsulated azide complex, Mn(salen)N_3, was prepared starting from Mn(salen)−Y and treatment with trimethylsilyl azide ($TMSN_3$) as previously reported (see Scheme 1).[27,28] After removal of the excess of ligand by Soxhlet extraction in dichloromethane for 8 h, the encapsulated complexes were ion exchanged with an aqueous 1M NaCl solution for 12 h to reduce the amount of residual tetrahedral Mn(salen) complex.

The encapsulated complex was characterized by comparison of its diffusion reflectance UV−vis (DR) and infrared (IR) spectra with those of the nonsupported complex, Mn^{III}(salen)-N_3, synthesized independently as reported in the literature.[29] FT-IR and DR spectra were obtained using the equipment and procedures previously reported.[28] The most salient spectroscopic features supporting the formation of Y zeolite-encapsulated Mn(salen)N_3 were a characteristic imine stretching vibration at 1615 cm^{-1}, a band typical of metallosalen complexes at 1535 cm^{-1}, and a sharp peak at 2037 cm^{-1} due to the azide ligand. The most relevant feature of DR spectrum is that the encapsulated complex presents a fluorescent emission which is entirely absent in the isolated Mn(salen)N_3 complex. A weak and broad emission band around 600 nm is observed whose excitation spectra are compatible with the DR absorption of azides.[28]

Paraloid B72, an ethyl methacrylate−methyl acrylate (70%/30%) copolymer (P[EMA/MA]) was used for PFE preparation because of its mechanical stability and ability to form uniform thin films on all kinds of substrates. The use of poly(methyl)-methacrylate films has been recommended for electrode modification in stripping analysis.[30] This polymer provides porous coatings that adheres the solid microparticles to the electrode surface,[31,32] thus facilitating the direct contact between the zeolite microparticles and the substrate electrode, which, according to Calzaferri et al.,[21] is a crucial aspect for studying the electrochemistry of zeolite-associated species. This can be seen in Figure 1, in which a SEM image of a zeolite-modified electrode is presented. This has been obtained using the equipment already described.[31,32]

Zeolite-modified electrodes (ZMEs) were prepared following the procedure devised by several authors,[25,33−36] by transferring 40−100 μL of a dispersion of the zeolite (10 mg) and graphite powder (10 mg) in acetone (5 mL) to the surface of freshly polished glassy carbon electrode and allowing the coating to dry in air. Then, one drop of a solution of the acrylic resin (1%) in acetone was added and the modified electrode was air-dried. The coatings examined contained 0.2−1.5 mg cm^{-2} of the dry zeolite. A platinum gauze pseudoreference electrode was used in organic solvents, whereas a saturated calomel electrode (SCE) was used as a reference electrode in experiments in aqueous solution. All the potentials reported here are referred to the aqueous SCE. A platinum-wire auxiliary electrode completed the electrode arrangement. Experiments were conducted using $LiNO_3$, $NaNO_3$, NaCl, Et_4NClO_4, and $NaClO_4$ as supporting electrolytes.

The zeolite powders were prepared, unless stated, by conditioning with slight grinding of zeolite probes. A series of abrasion-modified electrodes were also prepared by powdering 10 mg of the zeolite in an agata mortar and pressing a portion

on the electrode surface with a hard spatula to produce a spot of finely dispersed material. This spot was further covered by a Paraloid B72 coating. A similar procedure was used to prepare electrodes modified by dry Mn(salen)X (X = Cl, N_3) complexes.

Electrochemical measurements were performed in a conventional three-electrode thermostated cell under argon atmosphere. Linear scan and differential pulse voltammograms at low scan rates (v < 50 mV/s) were performed with a Metrohm E506 Polarecord, whereas cyclic voltammograms were carried out with a BAS CV-50W voltammetric analyzer, the potential scan rate ranging from 1 to 500 mV/s. Unless stated, electrochemical experiments were performed at 298.0 ± 0.5 K.

All reported peak potentials and currents were the mean value from three independent voltammograms. In almost all cases, uncertainties were 5 mV for peak potential values. In a few cases, uncertainties larger than 5 mV were obtained, and five independent measurements were carried out. Reproducibility tests were routinely carried out; prior to the series of runs, cyclic voltammograms of an aqueous solution (1.0 mM) of $K_4Fe(CN)_6$ (Merck) were performed at the unmodified GCE.

3. Results and Discussion

3.1. Electrochemistry of PFEs. The electrochemistry of Mn^{III}(salen) in solution (MeCN, DMSO) is well-known.[10,37,38] It consists essentially on a reversible one-electron process at a formal potential close to −0.20 V versus SCE. An identical electrochemical response was reported for the zeolite-associated complex in pressed graphite powder composite electrodes immersed into MeCN and DMSO.[9]

The electrochemical response obtained for Mn(salen)N_3 and Mn(salen)Cl complexes in aqueous solution (in concentrations in the range 10^{-3}−10^{-4} M) was entirely similar to that recorded in nonaqueous media. The formal electrode potential, calculated as the half sum of the cathodic and anodic peak potentials, is close to −0.28 V versus SCE regardless the concentration of the complex and the type and concentration of the supporting electrolyte.

Cyclic voltammograms for dry powders of Mn(salen)N_3 and Mn(salen)Cl complexes attached to PFEs immersed in aqueous media were similar to those recorded for complexes in solution. As shown in Figure 2a, the cyclic voltammogram for a Mn(salen)N_3−PFE immersed into a neutral aqueous solution exhibits a single one-electron reversible couple (C_1/A_1) whose formal electrode potential equals to −0.28 V versus SCE. No variations were observed in the peak potentials as a function of the supporting electrolyte.

No adsorption effects were detected, and the voltammetric parameters are nearly identical to those for complexes in solution. Although one can expect that a thin-layer behavior was operative for electrode-confined complexes, it appears that the large porosity of the polymer had facilitated the dissolution of the solid complex and then a diffusion-controlled response was obtained.

The cyclic voltammetric response of ZMEs of Y zeolite-associated Mn(salen)N_3 in aqueous media in the +0.4 to −0.6 V versus SCE potential range was similar to that of complexes in solution or solid complexes attached to PFEs. As shown in Figure 2b, only a well-defined couple, that can be assigned to the C_1/A_1 process, appears. The equilibrium potential of this couple, near to −0.25 V versus SCE, is slightly but consistently shifted with respect to that electrode process for complexes in solution.

As described in detail elsewhere,[39] this couple is accompanied by a pronounced anodic peak at +0.30 V (A_2) which can be attributed to a two-electron oxidation involving the azide group. This anodic process is depicted in Figure 3.

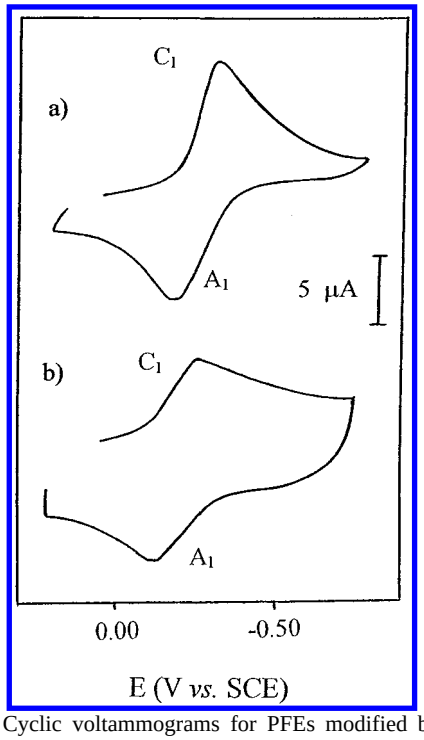

Figure 2. Cyclic voltammograms for PFEs modified by (a) solid Mn(salen)N_3 and (b) Y zeolite-associated Mn(salen)N_3. 0.15 M $NaClO_4$. Potential scan rate, 50 mV/s.

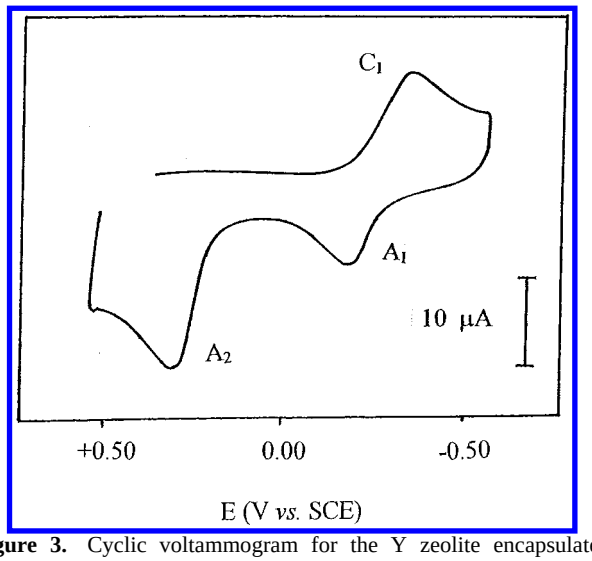

Figure 3. Cyclic voltammogram for the Y zeolite encapsulated Mn(salen)N_3 complex in the potential range from +0.5 to −0.5 V versus SCE. 0.15 M $NaClO_4$ aqueous solution. v = 50 mV/s.

The observed electrochemical behavior can be rationalized on the light of the current ideas on the electrochemistry of zeolite-entrapped systems assuming that the electron transfer proceeds only for electroactive species at the boundary of the solid. Then, the C_1 cathodic process can correspond to the reduction of Mn(salen)N_3 complexes existing in solution after eventual leaching of zeolite-encapsulated ones or located in the external boundary sites of the zeolite. In the first case, the redox process equals to that in solution:

$$Mn^{III}(salen)N_{3(sol)} + e^- = Mn^{II}(salen)N_3^-{}_{(sol)} \qquad (1)$$

The reduction of boundary-associated complexes can yield species in solution

$$Mn^{III}(salen)N_{3(b)} + M^{+}_{(sol)} + e^{-} = Mn^{II}(salen)N_3^{-}{}_{(sol)} + M^{+}_{(b)} \quad (2)$$

or involve the electron-transfer process to a zeolite-associated species:

$$Mn^{III}(salen)N_{3(b)} + M^{+}_{(sol)} + e^{-} = Mn^{II}(salen)N_3^{-}{}_{(b)} + M^{+}_{(b)} \quad (3)$$

where (sol) represents species in the solution phase and (b) boundary-associated species. M^+ represents the charge-balancing cation of the supporting electrolyte.

The subsequent oxidation of the boundary-associated Mn(II) species (process A_1) can proceed via the inverse of process 3:

$$Mn^{II}(salen)N_3^{-}{}_{(b)} + M^{+}_{(b)} = Mn^{III}(salen)N_{3(b)} + M^{+}_{(sol)} + e^{-} \quad (4)$$

and/or via generation of Mn(III) species in solution

$$Mn^{II}(salen)N_3^{-}{}_{(b)} + M^{+}_{(b)} = Mn^{III}(salen)N_{3(sol)} + M^{+}_{(sol)} + e^{-} \quad (5)$$

followed eventually by ligand loss and aquation reactions.

3.2. Topological Redox Isomers. When comparing the electrochemical data for the reduction of solid Mn^{III}(salen)X (X = Cl, N_3) complexes in solution or attached to PFEs and Y zeolite-associated Mn(salen)N_3, one observes some significant differences. This is illustrated in Figure 4a, in which LSVs for Mn(salen)Cl in solution (0.15 M Et_4NClO_4) and a PFE modified by lightly ground Mn(salen)N_3 containing zeolite are compared. For Mn^{III}(salen)X complexes in solution as well as for such solid complexes atached to PFEs, voltammograms fit to theoretical $i-E$ curves for a one-electron reversible transfer controlled by diffusion,[40] eventually incorporating a correction due to uncompensated ohmic drop associated to the polymer film.[41] In contrast, voltammetric curves for zeolite-associated Mn(salen)N_3 present a tall morphology, with a relatively fast decay at potentials past the peak that refers to the thin-layer behavior.[42]

These data suggest a dual response as also indicated by differential pulse voltammograms. As can be seen in Figure 4b, at low scan rates, two overlapped voltammetric peaks appear. This apparently dual response also appears on comparing the dependence of the peak potentials of the C_1/A_1 couple on the potential scan rate v. Thus, for a diffusion-controlled reversible electron-transfer process the cathodic and anodic peak potentials must be separated 59 mV regardless the potential scan rate. The peak potential separation ($E_{pc}-E_{pa}$) must be zero at all scan rates for a reversible electron transfer involving reactants strongly confined to the electrode surface.[42]

As depicted in Figure 5, for solid Mn(salen)X complexes attached to PFEs as dry powder, the peak potential separation increases slowly on increasing v and tends to the theoretical value for a reversible one-electron transfer (59 mV) at zero scan rates.[40,41] The formal electrode potential, $E^{0\prime}$ (calculated as the half sum of the peak potentials), however, remains identical at all scan rates. This behavior agrees with that expected for electron-transfer processes with a small uncompensated ohmic drop. This is confirmed by the fact that the peak to half peak potential separation ($E_p-E_{p/2}$) and the cathodic to anodic peak

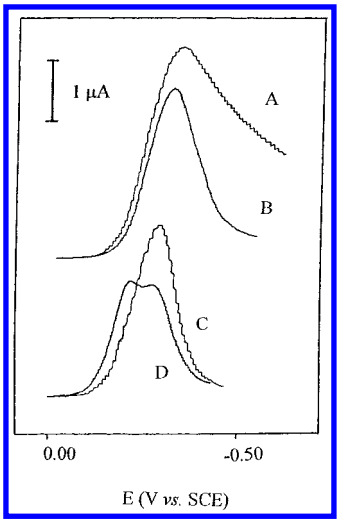

Figure 4. Linear scan voltammograms at $v = 5$ mV/s. (A) A solution of Mn(salen)Cl (0.45 mM) in 0.10 M Et_4NClO_4 using an unmodified GCE; (B) PFE modified by Y zeolite-associated Mn(salen)N_3 complex immersed into 0.10 M Et_4NClO_4.

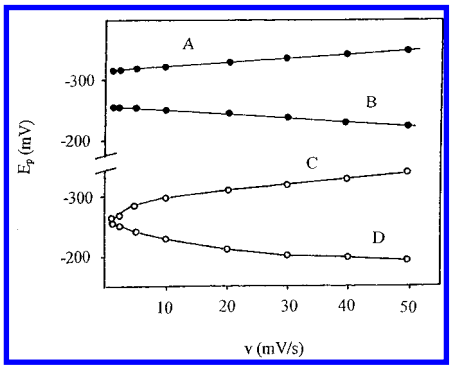

Figure 5. (a) Variation of the cathodic (A,C) and anodic (B,D) peak potentials of the C_1/A_1 couple on the potential scan rate for PFEs modified by solid Mn(salen)Cl (points) and Y zeolite-associated Mn(salen)N_3 (circles). Supporting electrolyte 0.10 M $NaNO_3$.

potential separation ($E_{pc}-E_{pa}$) tend to the expected value for a reversible one-electron transfer (59 mV) for films containing 0.2 mg/cm^2 of polymer. In contrast, for zeolite-associated Mn(salen)N_3 complexes, the peak potential separation decreases rapidly at low scan rates and apparently tends to zero at zero scan rates, as also shown in Figure 5. This behavior refers to the voltammetric pattern observed in voltammetry of reactants confined to the electrode surface for which $E_{pc} = E_{pa}$ (vide infra).[42] Interestingly, the formal electrode potential at scan rates larger than 20 mV/s are consistently more negative than those measured at scan rates below 20 mV/s.

On the other hand, the formal electrode potential of the C_1/A_1 couple of Mn^{III}(salen)X (X = Cl, N_3) complexes in solution becomes almost entirely independent of the nature and concentration on the supporting electrolyte at all scan rates (from 1 to 500 mV/s). Identical result was obtained for electrodes modified by powdered solid complexes.

In contrast, the value of the formal electrode potential for Mn(salen)N_3-associated zeolite-modified electrodes depends on the supporting electrolyte and its concentration. This can be seen in Figure 6, in which the calculated formal potentials for Mn(salen)Cl in solution (A,B) and for Y zeolite-associated Mn(salen)N_3 (C,D) in $LiNO_3$ electrolytes have been represented at two different scan rates as a function of the concentration of the supporting electrolyte. The influence of the nature of the electrolyte is summarized in Table 1, in which formal electrode

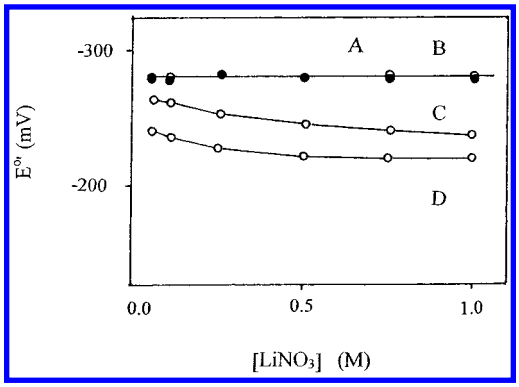

Figure 6. Variation of the formal electrode potential of the C_1/A_1 couple for Mn(salen)Cl in solution (A,B) and for Y zeolite-associated Mn(salen)N_3 (C,D) on the concentration of $LiNO_3$. Points, data at 5 mV/s; circles, data at 20 mV/s.

TABLE 1: Formal Electrode Potentials, Free Energy, Enthalpy, and Entropy for Electrode Processes Involving Mn(Salen)X (X = Cl, N_3) Complexes in Solution and Y Zeolite-Associated Mn(salen)N_3[a]

system	electrolyte	$E^{\circ\prime}$ (mV vs SCE)	ΔG°_{MnY} (kJ/mol)	ΔH°_{MnY} (kJ/mol)	ΔS°_{MnY} (J mol^{-1} K^{-1})
Mn(salen)Cl (sol)	[b]	−285(5)	+4.15(5)	+4.15(5)	0.0(2)
Mn(salen)N_3 (sol)	[b]	−275(5)	+3.18(5)	+3.18(5)	0.0(2)
(i) Mn(salen)N_3−Y	$LiNO_3$	−265(5)	+2.22(4)	+3.2(3)	+18(1)
(i) Mn(salen)N_3−Y	$NaNO_3$	−260(5)	+1.74(3)	+5.7(4)	+25(1)
(i) Mn(salen)N_3−Y	Et_4NClO_4	−255(5)	+1.25(3)	+11.9(6)	+44(2)
(ii) Mn(salen)N_3−Y	$LiNO_3$	−235(5)	−0.68(2)	+1.4(3)	+7(1)
(ii) Mn(salen)N_3−Y	$NaNO_3$	−225(5)	−1.64(3)	+0.7(3)	+8(1)
(ii) Mn(salen)N_3−Y	Et_4NClO_4	−215(5)	−2.60(5)	+0.4(3)	+10(1)

[a] $E^{\circ\prime}$ values calculated as the half-sum of the peak potentials measured in voltammograms of modified electrodes at different electrolytes (all in concentrated 0.10 M). Data at 1 mV/s were ascribed to isomer i, and data at 20 mV/s were taken for evaluating the thermochemical parameters of isomer ii. Number in parentheses represent the uncertainty in the last significant figure. [b] Identical values in all three electrolytes.

potentials calculated from CVs at 1 and 20 mV/s in $LiNO_3$, $NaNO_3$, and Et_4NClO_4 electrolytes are listed. In all cases, a small but consistent difference exists between the formal electrode potential of the complex Mn(salen)N_3 in solution at any potential scan rate and those calculated for Y zeolite-associated Mn(salen)N_3 at low and high scan rates. These results indicate that for ZMEs the overall electrode process depends on the nature of the positive ion of the supporting electrolyte, as expected for an electrochemical mechanism mediated by the ingress of a counterion from the solution into the zeolite (eqs 1−5).

In this context, the Tafel plots obtained from $i-E$ data in the rising portion of voltammetric curves also reveal a significant difference between ZMEs and the complexes in solution. As shown in Figure 7, for Mn(salen)N_3 complexes in solution or attached to PFEs, a linear dependence of ln$i$ on E was obtained. In contrast, zeolite-associated Mn(salen)N_3 provided Tafel plots apparently formed by two differentiated regions.

The amount of accessible manganese sites can be estimated from the quantities of charge passed in the peaks during the linear scan voltammograms. The number of electroactive centers can be calculated using Faraday's law by integrating the charge under the voltammetric waves. For modified electrodes typically containing 0.10 mg of zeolite, net amounts of charge ranging from 8 to 10 μC were passed depending on the zeolite mechanical treatment. Since the total complex concentration into the zeolite was 0.48%, one finds that only 0.9% of the zeolite-

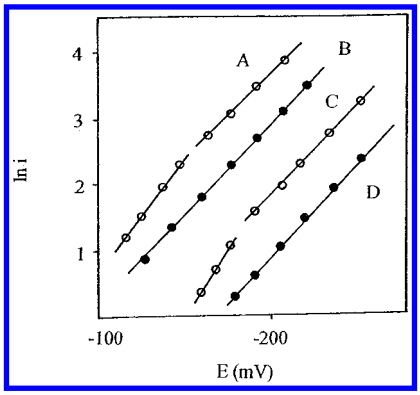

Figure 7. Comparison of Tafel plots for Y zeolite-associated Mn(salen)N_3 PFEs at 70 (A) and 23 °C (C) and for Mn(salen)N_3 in solution at 70 (B) and 23 °C (D). From linear scan voltamograms at 20 mV/s. Supporting electrolyte, 0.10 M $NaNO_3$.

encapsulated complex was electroactive. This result indicates that the observed electrochemistry corresponds essentially to Mn(salen)N_3 complexes in the boundary sites of the zeolite.

All these data suggest the coexistence of two different topological redox isomers attached to the zeolite boundary, i.e., two different electroactive centers consisting on the same complex associated or located differently with the host. On first examination, these can be considered as (i) a "more external" isomer for which the equilibrium potential is near to −0.25 V, and (ii) a "less external" isomer whose equilibrium potential appears near to −0.20 V (vide infra).

This idea is consistent with the variation of such electrochemical response on the mechanical work imparted to the sample (from mild grinding to abrasive conditioning) and the time in which the modified electrode remains immersed into the electrolyte solution prior to the electrochemical runs (rest time) as reported by different authors.[25,36]

Thus, upon abrasive conditioning of zeolites, the voltammetric profil of C_1 at zero rest times slightly approaches to that of isomer ii overlapped with that of Mn(salen)N_3 complex in solution. Since abrasive treatments may break the zeolite aggregates into smaller particles and also create cracks and crevices on the particles, the electrochemistry observed for abrasive-conditioned ZMEs must correspond mainly to that of the "more external" Mn(salen)N_3 topological redox isomer eventually superimposed with that of a small amount of complexes passing to the solution.

For lightly ground conditioned zeolites, the electrochemical behavior is sensitive to potential scan rate and the time of contact of the electrode with the electrolyte solution. At contact times less than 5 min, and at relatively high scan rates (v > 10 mV/s), peak C_1 looks like a difusion-controlled process. However, on increasing contact time, the peak potential decreases, and a fast decay of the current after the voltammetric peak is again observed, thus denoting that the response associated to the "less external" isomer ii predominates. Consistently, blank experiments on Mn(salen)N_3-associated zeolites that have been previously dispersed in solution provided extremely weak electrochemical signals for complexes in solution, denoting that a very limited leaching process exists. The resulting zeolite-modified electrodes weak responses close to the thin-layer behavior.

In agreement with the foregoing considerations, the electrochemistry of the "more external" boundary-associated redox isomer can in principle be described as a one-electron reduction controlled by the diffusion of the electrolyte countercation in the channels/windows system of the zeolite matrix. On first examination, one can use the model described by Baker et

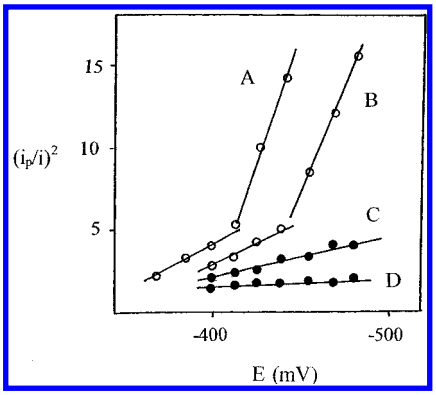

Figure 8. Cottrell-type representations corresponding to the diffusive region of LSVs (v = 20 mV/s) for Y zeolite-associated Mn(salen)N_3 modified electrode at 70 (A) and 23 °C (B) and for Mn(salen)Cl in solution at 70 (C) and 23 °C (D). Supporting electrolyte 0.10 M $NaNO_3$.

al.[15−18] for zeolites containing relatively mobile Na^+ and Ag^+ ions. In this case and assuming semi-infinite diffusion on the zeolite bulk, a reversible diffusion-controlled behavior can be expected so that the peak current can be calculated as

$$i_p = 0.4463nFAc^*(nF/RT)^{1/2}v^{1/2}D^{1/2} \quad (6)$$

where c^* represents the concentration of electroactive species in the bulk of the zeolite and D the intrazeolitic counterdifusion coefficient. Strictly, this coefficient reflects the mobility of electroactive species and the charge-balancing electrolyte cation in the channel network. A is the electrode area, and the other symbols have their usual meaning. For this kind of process, it can be expected that the diffusion-controlled portion of the voltammetric curve (from 100 to 150 mV past the peak) verifies the Cottrell equation:

$$i = nFAc^*D^{1/2}/(\pi t)^{1/2} \quad (7)$$

which, for a linear sweep experiment, can be rewriten as:[43,44]

$$1/i^2 = \pi E_{dif}/(nFAc^*)^2Dv - \pi E/(nFAc^*)^2Dv \quad (8)$$

where E_{dif} represents the potential at which the diffusive behavior starts. This equation predicts a linear dependence of $1/i^2$ on potential for the diffusive portion of voltammograms. In addition, if the electrode area and the concentration of the electroactive species are known, one can estimate the value of the diffusion coefficient D.

As expected, for experiments on the complexes Mn(salen)X (X = Cl, N_3) in solution, the diffusion coefficients calculated from peak potential data using eq 6 were in excellent agreement with those calculated from the Cottrell-type analysis of voltammetric curves derived from eq 10 (typical values, 4.6×10^{-5} cm^2/s at 298 K).

To compare data in solution with those for zeolite-associated species, it is convenient to use the normalized $(i_p/i)^2$ ratio:

$$(i_p/i)^2 = 0.6258(nF/RT)(E_{dif} - E) \quad (9)$$

This can be seen in Figure 9, in which plots of $(i_p/i)^2$ versus E for a solution of Mn(salen)Cl ((0.10 M $NaNO_3$) at 23 (A) and 70 °C (B) are depicted.

On the contrary, for zeolite-associated complexes, two different regions can be distinguished in $(i_p/i)^2$ versus E plots. This is in agreement with the observed "fast" decay of the current passing the voltammetric peak on comparing the voltammograms of zeolite-associated complexes with those of

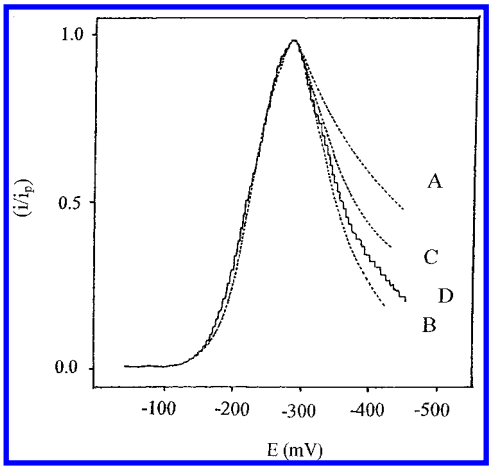

Figure 9. Comparison of theoretical normalized $i-E$ curves (A−C) and experimental LSV (D) at 20 mV/s for Y zeolite-associated Mn(salen)N_3 modified electrodes. (A) reversible diffusion-controlled process and (B) a reversible electron transfer for an electroactive species attached to the electrode surface. Both calculated for $E^{\circ\prime} = -250$ mV. Curve C was calculated as the sum of independent processes A and B with contributions of 70% and 30%, respectively.

complexes (solid or in solution phase), as can be seen in Figure 4a. Since for zeolite-modified electrodes it is not possible to know the values of the effective electrode area, concentration of depolarizer, and the counterdiffusion coefficient, only the $Ac^*D^{1/2}$ terms calculated as before from eqs 6 and 8 can be compared. Interestingly enough, the values of such term calculated from peak potential data were also in excellent agreement with those calculated from the slope of the region close to the voltammetric peak in $1/i^2$ versus E plots.

This behavior must be superimposed to the weaker response of a second topological redox isomer which is strongly attached to the zeolite boundary. Its electrochemistry can in principle be treated as that described for electroactive species confined to the electrode surface. Assuming reversibility, voltammetric curves must verify[44]

$$i = \frac{n^2F^2vA\Gamma_{ox}(b_{ox}/b_{rd})\exp[nF(E - E^{\circ\prime})/RT]}{RT\{1 + (b_{ox}/b_{rd})\exp[nF(E - E^{\circ\prime})/RT]\}^2} \quad (10)$$

where Γ_{ox} is the surface concentration of the oxidized form of electroactive species and the coefficients b_i (i = ox, rd) are equal to $\Gamma_i \exp(-\Delta G_i^\circ/RT)$, ΔG_i° being the standard free energy of surface attachment. For strongly adsorbed reactants and products, this model predicts symmetrical voltammetric curves with $E_{pc} = E_{pa} = E^{\circ\prime} + (RT/nF)\ln(b_{ox}/b_{rd})$ and the peak current given by

$$i_p = n^2F^2vA\Gamma_{ox}/4RT \quad (11)$$

From the foregoing set of equations, theoretical $i/i_p = f(E)$ curves can be predicted for electrode processes involving both topological redox isomers. In Figure 9, normalized curves have ben plotted for a one-electron diffusion-controlled process (A) and a strongly electrode-attached electroactive species (B) and for a combination of both, assuming that the strongly attached isomer is present in a 30−35% of the total electroactive species (curve C). The voltammetric profil in this last case is close to that experimentally obtained (curve D). The best fit of theoretical curves with experimental LSVs is obtained inserting $E^{\circ\prime}$(isomer i) = −0.25 V versus SCE and $E^{\circ\prime}$(isomer ii) = −0.20 versus SCE, as can be seen in Figure 10.

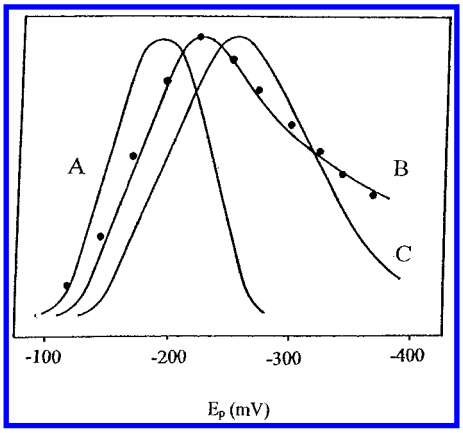

Figure 10. Normalized $i-E$ curves for a electrode-attached species (A) and for a combination of the same with $E^{o\prime} = -200$ (B) and -250 mV (C) with a diffusion-controlled process (50% contribution) with $E^{o\prime} = -250$ mV. Points correspond to experimental data for a Y zeolite-associated Mn(salen)N_3 modified electrode at 10 mV/s for in 0.15 M $NaClO_4$.

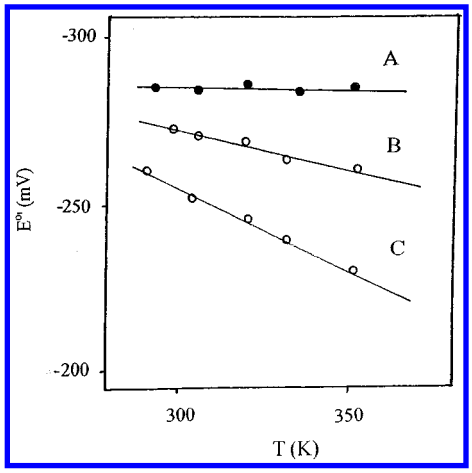

Figure 11. Temperature dependence of the formal electrode potential of the C_1/A_1 couple for (A) Mn(salen)Cl in solution (0.10 M $NaNO_3$), (B) Y zeolite-associated Mn(salen)N_3 modified electrode immersed into 0.10 M $NaNO_3$), and (C) Y zeolite-associated Mn(salen)N_3 modified electrode immersed into 0.10 M Et_4NClO_4. From CVs at 20 mV/s.

In this context, one can expect that high v values promote the response of the 'less external' isomer for which a thin-film behavior (with peak current proportional to v) is expected. On the contrary, the use of low v values must enhance the response of the "more external" isomer, for which a diffusion-controlled response (peak current proportional to $v^{1/2}$) is operative. Contrary to these expectances, the thin-layer behavior prevailed at low scan rates.

This can be rationalized on considering that in the studied system, bulky Mn(salen)N_3 complexes are encapsulated into zeolite Y. In contrast with Na^+- and Ag^+-containing zeolites studied in refs 15−18, electrochemically accessible Mn(salen)-N_3 complexes are probably confined to a narrow region of the zeolite grains, as indicated by the net amount of charge passed under voltammetric peaks. Then, although illustrative of the different electrochemistry of i and ii redox isomers, the diffusive model represented by eqs 6−10 only provides a weak approach to the existing conditions in Mn(salen)N_3 zeolites.

In this context, the different amount and accessibility of boundary-confined complexes are responsible for the different electrochemical response of i and ii redox isomers. In agreement with repetitive voltammetry data, electrochemically accessible complexes must be exhausted in time during electrochemical runs. Accordingly, it is in principle concevaible that the observed electrochemistry conforms with that of isomer i at relatively high scan rates (short times) whereas the observation of isomer ii is favored at low scan rates (large times). This situation is close to that recently described by Baker et al. on Ag^+-containing zeolite Y, in which the zeolite is rapidely depleted of silver and semi-infinite diffusion occurs only in a few seconds at the beginning of electrochemical experiments.[45]

Thus, "entirely external complexes", passing from the zeolite to the solution from broken surface cages, must produce an electrochemical response that probably equals that in solution. Peak potentials should be almost independent of the potential scan rate and almost electrolyte-independent; voltammetric curves curves should exhibit a diffusive behavior.

With regard to boundary-associated isomers, one can discern: (i) A "weakly boundary-associated isomer" or "external isomer", for which the electrochemical process is at least initially controlled by the diffusion of electrolyte countercations through the zeolite system. Peak potentials should be sweep rate-dependent and electrolyte-dependent, but voltammetric curves present a diffusion-controlled profile.

(ii) A "less external isomer" or "strongly boundary-asociated isomer", for which a voltammetric behavior close to that of thin-layer cells is operative. This is probably constrained by the conditions of attachement of the electroactive species to the zeolite boundary but also on the diffusion of electrolyte cations in the zeolite channels and windows.

3.3. Evaluation of Kinetic and Thermochemical Parameters. To obtain more information on the differences between the zeolite-associated topological redox isomers, the temperature dependence of the electrochemical parameters has been studied in the range from 0 to 80 °C. Assuming an Arrhenius dependence of the counterdiffusion coefficient,[46] one can determine the activation energy associated with the diffusion step, provided that it is rate limiting, as the slope of the ln i_p versus $1/T$ plots. Using the peak current values for C_1 at large scan rates, in which apparently the response of the redox isomer i prevails, linear dependences between ln i_p and $1/T$ were obtained. As expected, the apparent activation energy, E_{dif}, calculated from those representations varied with the electrolyte, with values of 22 ± 1 kJ/mol (0.10 M $LiNO_3$), 37 ± 2 kJ/mol (0.10 M $NaNO_3$), and 47 ± 2 kJ/mol (0.10 M Et_4NClO_4). The estimated values of E_{dif} for Y zeolite associated Mn(salen)N_3 are close to that calculated by Barker et al. for the intrazeolite counterdiffusion coefficient for silver−sodium cations in the large channel network of zeolite Y (30 ± 1 kJ/mol) and for the intracrystalline ion exchange (35 ± 1 kJ/mol).[17] Large activation energies for self-diffusion of intrazeolite cations have been observed and interpreted in terms of intrazeolite diffusion controlling the rate of ion exchange.[47] As expected, the activation energy for the counterdiffusion process increases as the size of the mobile cation increases ($Li^+ < Na^+ < Et_4N^+$).

As shown in Figure 11, the formal potential for Mn(salen)X complexes in solution is almost independent of temperature, whereas for PFEs modified by zeolite-associated Mn(salen)N_3 complexes, a significant variation is observed. To estimate thermochemical data, formal electrode potentials for Y zeolite-associated Mn(salen)N_3 complexes in different electrolytes have been calculated as the half sum of the peak potentials. The peak potential values in LSVs recorded at 1 mV/s and 20 mV/s have been used, respectively, for assigning the formal electrode potentials to the ii and i isomers. Although uncompensated ohmic drops distort the voltammetric response, the absence of coupled chemical reactions and the use of relatively low scan

SCHEME 2: Thermochemical Cycle for Electron Transfer Processes Involving Y Zeolite-Associated Mn(Salen)N_3 Topological Redox Isomers

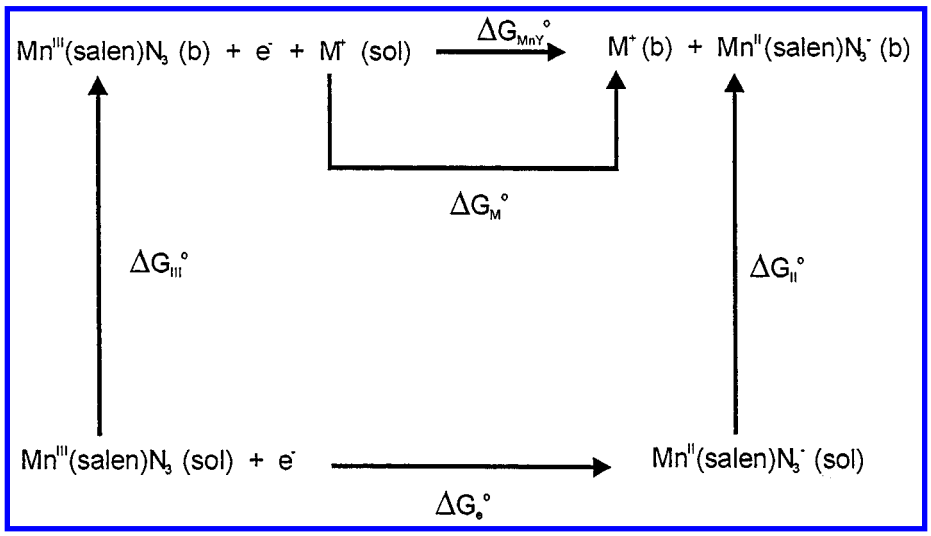

TABLE 2: Differences in Free Energy, Enthalpy, and Entropy for Electrode Processes Involving Mn(salen)N_3 Complexes in Solution and Associated to Y Zeolite[a]

system	electrolyte	$(\Delta G°_{MnY} - \Delta G°_e)$ (kJ/mol)	$(\Delta H°_{MnY} - \Delta H°_e)$ (kJ/mol)	$(\Delta S°_{MnY} - \Delta S°_e)$ (J mol^{-1} K^{-1})
(i) Mn(salen)N_3−Y	$LiNO_3$	−0.96(4)	0.0(4)	+18(1)
(i) Mn(salen)N_3−Y	$NaNO_3$	−1.44(5)	+2.5(5)	+25(1)
(i) Mn(salen)N_3−Y	Et_4NClO_4	−1.93(5)	+8.7(7)	+44(2)
(ii) Mn(salen)N_3−Y	$LiNO_3$	−3.86(6)	−1.8(4)	+7(1)
(ii) Mn(salen)N_3−Y	$NaNO_3$	−4.84(6)	−2.5(5)	+8(1)
(ii) Mn(salen)N_3−Y	Et_4NClO_4	−5.78(6)	−2.8(5)	+10(1)

ii−i		$\Delta\Delta G°_{MnY}$ (kJ/mol)	$\Delta\Delta H°_{MnY}$ (kJ/mol)	$\Delta\Delta S°_{MnY}$ (J mol^{-1} K^{-1})
Mn(salen)N_3−Y	$LiNO_3$	−2.90(5)	−1.8(4)	−11(2)
Mn(salen)N_3−Y	$NaNO_3$	−3.38(4)	−5.0(5)	−17(2)
Mn(salen)N_3−Y	t_4NClO_4	−3.85(6)	−11.5(8)	−34(3)

[a] From voltammetric data at 20 mV/s for isomer i and at 1 mV/s for isomer ii on zeolite-modified electrodes immersed into different electrolytes (all in concentrated 0.10 M). Number in parentheses represent the uncertainty in the last significant figure.

rates make reasonable the use of the half sum of peak potentials for calculating the formal electrode potential.[48−50] Experimental data fit to linear dependences of $E°'$ on temperature, enabling for a direct estimate of the free energy, enthalpy, and enthropy for the electrochemical process. All these parameters are summarized in Table 1. The temperature dependence of the electrochemical parameters has been studied in the range from 0 to 80 °C. As shown in Figure 10, the formal potential for Mn(salen)X complexes in solution is almost independent of temperature, whereas for PFEs modified by zeolite-associated Mn(salen)N_3 complexes, a significant variation is observed. Experimental data fit to linear dependences of $E°'$ on temperature, enabling for a direct estimate of the free energy, enthalpy, and enthropy for the electrochemical process. All these parameters are summarized in Table 1.

As depicted in the thermochemical cycle in Scheme 2, the overall redox process involving a zeolite-associated Mn(salen) complex can be related with the solution/zeolite boundary interchange of both Mn(III) and Mn(II) complexes, the interchange of the charge-compensating cation from the supporting electrolyte, and the redox process in solution phase. This scheme is in principle valid for both topological redox isomers i and ii.

Accordingly, the free energy of the overall redox process for zeolite-associated species, $\Delta G°_{MnY}$, can be expressed as the sum of the standard free energy for the electron-transfer step in solution, $\Delta G°_e$, the standard free energy of the transfer of the charge compensating counterion, $\Delta G°_M$, and the standard free energy associated to the transfer of Mn(III) and Mn(II) complexes from the solution to the zeolite boundary, $\Delta G°_{III}$ and $\Delta G°_{II}$:

$$\Delta G°_{MnY} = \Delta G°_e + \Delta G°_M - \Delta G°_{III} + \Delta G°_{II} \qquad (12)$$

assuming that no changes in the direct coordination arrangement of the electroactive center occur. Obviously, similar relationships hold for enthalpy and entropy. The above condition is unambiguously accomplished by Mn(salen)N_3 complexes for which the values of $\Delta G°_{MnY}$ and $\Delta G°_e$ can easily be calculated from the formal electrode potentials that are different for each of the two topological redox isomers. The corresponding values of free energy, enthalpy, and entropy estimated for topological redox isomers i and ii are also summarized in Table 1.

The term $\Delta G°_{MnY}$ corresponds to the free energy of the overall electrode process described by eq 3, applicable to both i and ii redox isomers. The difference $(\Delta G°_{MnY} - \Delta G°_M)$ is the representative of the different stability of the oxidized and reduced forms of boundary-associated complexes, i.e., the free energy for the process Mn(salen)N_3 (b) + e^- = Mn(salen)N_3^- (b).

Interestingly, a comparison of the differences $(\Delta G°_{MnY} - \Delta G°_M)$ is representative of differences in $\Delta G°_M$ for the transfer of Li^+, Na^+, and Et_4N^+ ions from the solution to the zeolite system. The calculated values are listed in Table 2. Contrary to that expected, the spontaneity of the overall redox process increases from Li^+ to Et_4N^+ countercations. This result must be related with the fact that cations must partially desolvate in

order to pass through the zeolite pores.[19] Finally, the difference in the value of ΔG°_{MnY} for both topological redox isomers can be considered as representative of the relative stability of such isomers with regard to their transfer from the solution phase to the zeolite boundary. The calculated values are also shown in Table 2. As expected, the topological redox isomer ii exhibits a thermochemical stability larger than that of the topological redox isomer i. The differences $\Delta\Delta G^\circ_{MnY}$ ($= \Delta G^\circ_{MnY}$ (ii) $- \Delta G^\circ_{MnY}$ (i)) are strongly dependent on the electrolyte countercation, denoting that the ingress/issue of electrolyte ions from/to the solution plays an important role in the overall electrochemical process described by eq 12.

4. Conclusions

The use of polymer film electrodes allows to record well-defined electrochemical responses for Y zeolite-associated Mn(salen)N_3 immersed not only into organic solvents but also into aqueous solutions. The electrochemical response depends significantly on the mechanical conditioning of the zeolite samples and the positive counterions of the supporting electrolyte. Current data on the voltammetry of zeolite-associated Mn(salen) can be described in terms of the coexistence of two different topological redox isomers: (i) a "more external" isomer, corresponding to a weakly boundary-associated Mn(salen)N_3 complex whose electrochemical response corresponds to a reversible one-electron-transfer controlled by diffusion of the positive ions of the supporting electrolyte through the zeolite surface windows and channels, and (ii) a "less external" isomer, corresponding to a strongly boundary-associated Mn(salen)N_3 complex for which the electrochemical response parallels that of reagents firmly attached to the electrode surface.

References and Notes

(1) Herron, N. *J. Coord. Chem.* **1988**, *19*, 25.
(2) Hanson, R. M. *Chem. Rev.* **1991**, *91*, 437.
(3) Jacobsen, E. N.; Zhang, W. *J. Org. Chem.* **1991**, *56*, 2296.
(4) Minutolo, F.; Pini, D.; Salvadori, P. *Tetrahedron Lett.* **1996**, *37*, 3375.
(5) Vankelecom, I. E. J.; Tas, D.; Parton, R. F.; Vandevyver, V.; Jacobs, P. A. *Angew. Chem., Int. Ed. Engl.* **1996**, *35*, 1346.
(6) Sabater, M. J.; Corma, A.; Doménech, A.; Fornés, V.; García, H. *J. Chem. Soc., Chem. Commun.* **1997**, 1285.
(7) Dutta, P. K.; Ledney, M. M. *Prog. Inorg. Chem.* **1997**, *44*, 209.
(8) Bedioui, F.; De Boysson, E.; Devynck, J.; Balkus, K. J., Jr. *J. Electroanal. Chem.* **1991**, *315*, 313.
(9) Bedioui, F. De Boysson, E.; Devynck, J.; Balkus, K. J., Jr. *J. Chem. Soc., Faraday Trans.* **1991**, *87*, 3831.
(10) Gaillon, L. Sajot, N.; Bedioui, F.; Devynck, J.; Balkus, K. J., Jr. *J. Electroanal. Chem.* **1993**, *345*, 157.
(11) Bedioui, F. Roué, L.; Briot, E.; Devynck, J.; Bell, S. L.; Balkus, K. J., Jr. *J. Electroanal. Chem.* **1994**, *373*, 19.
(12) Senaratne, C. Baker, M. D.; Zhang, J.; Bessel, C. A.; Rolison, D. R. *J. Phys. Chem. B* **1996**, *100*, 8610.
(13) Bedioui, F.; Devynck, J.; Balkus, K. J., Jr. *J. Phys. Chem.* **1996**, *100*, 8607.
(14) Rolison, D. R. Bessel, C. A.; Baker, M. D.; Senaratne, C.; Zhang, J. *J. Phys. Chem.* **1996**, *100*, 8610.
(15) Baker, M. D.; Zhang, J. *J. Phys. Chem.* **1990**, *94*, 8703.
(16) Baker, M. D. Senaratne, C.; Zhang, J. *J. Chem. Soc., Faraday Trans.* **1992**, *88*, 3187.
(17) Baker, M. D. Senaratne, C.; Zhang, J. *J. Phys. Chem.* **1994**, *98*, 1668.
(18) Baker, M. D. Senaratne, C.; McBrien, M. *J. Phys. Chem.* **1995**, *99*, 12367.
(19) Bedioui, F. *Coord. Chem. Rev.* **1995**, *144*, 39.
(20) Li, J-W.; Calzaferri, G. *J. Electroanal. Chem.* **1994**, *377*, 163.
(21) Li, J-W.; Pfanner, K.; Calzaferri, G. *J. Phys. Chem.* **1995**, *99*, 2119.
(22) Gemborys, H. A.; Shaw, B. R. *J. Electroanal. Chem.* **1986**, *95*, 208.
(23) Li, Z.; Mallouk, T. E. *J. Phys. Chem.* **1987**, *91*, 643.
(24) Li, Z. Wang, C. M.; Persaud, L.; Mallouk, T. E. *J. Phys. Chem.* **1988**, *92*, 2592.
(25) Bessel, C. A.; Rolison, D. R. *J. Phys. Chem. B* **1997**, *101*, 1148.
(26) Turro, N. J.; García-Garibay, M. In *Photochemistry in Organized Media*; Ramamurthy, V., Ed.; VCH: New York, 1991; pp 1−38.
(27) Doménech, A.; Formentín, P.; García, H.; Sabater, M. J. *Eur. J. Inorg. Chem.* **2000**, 1339.
(28) Formentín, P.; Folgado, J. V.; Fornés, V.; García, H.; Márquez, F.; Sabater, M. J. *J. Phys. Chem.* **2000**, *104*, 8361.
(29) Leighton, J. L.; Jacobsen, E. N. *J. Org. Chem.* **1996**, *61*, 389.
(30) Kaufmann, J. M.; Montenez, T.; Vandenvalck, J. L.; Patriarche, G. I. *Mikrochim. Acta* **1984**, *I*, 95.
(31) Doménech, A.; Doménech, M. T.; Gimeno, J. V.; Moyá, M.; Bosch, F. *Electroanalysis* **2000**, *12*, 120.
(32) Doménech, A.; Doménech, M. T.; Moya, M.; Gimeno, J. V.; Bosch, F.; *Anal. Chim. Acta* **2000**, *407*, 275.
(33) Ghosh, P. K.; A. W-Mau, H.; Bard, A. J. *J. Electroanal. Chem.* **1984**, *169*, 315.
(34) H-Liu, Y.; Anson, F. C. *J. Electroanal. Chem.* **1985**, *184*, 411.
(35) Li, J.; Calzaferri, G. *J. Chem. Soc., Chem. Commun.* **1993**, 1430.
(36) Horwitz, C. P.; Creager, S. E.; Murray, R. W. *Inorg. Chem.* **1990**, *29*, 1006.
(37) Bedioui, F.; Labbé, E.; Gutiérrez-Granados, S.; Devynck, J. *J. Electroanal. Chem.* **1991**, *301*, 267.
(38) Bedioui, F.; Roué, L.; Devynck, J.; Balkus, K. J., Jr. *Stud. Surf. Sci. Catal.* **1994**, *84*, 917.
(39) Doménech, A. Formentín, P.; García, H.; Sabater, M. J. submitted.
(40) Nicholson, R. S.; Shain, I. *Anal. Chem.* **1964**, *36*, 706.
(41) Nicholson, R. S. *Anal. Chem.* **1965**, *37*, 667.
(42) Bard, A. J.; Faulkner, L. R. *Electrochemical Methods*; John Wiley & Sons: New York, 1980.
(43) Ginzburg, G. *Anal. Chem.* **1978**, *50*, 375.
(44) Eggins, B. R.; Smith, N. H. *Anal. Chem.* **1979**, *51*, 2282.
(45) Baker, M. D.; McBrien, M.; Burgess, I. *J. Phys. Chem. B* **1998**, *102*, 2905.
(46) Dyer, A.; Fawcett, J. M. *J. Inorg. Nucl. Chem.* **1966**, *28*, 615.
(47) Barrer, R. M. *Pure Appl. Chem.* **1980**, *52*, 2143.
(48) Sawyer, D. T.; Chiericato, G.; Angelis, C. T.; Nanni, E. J.; Tsuchiya, T. *Anal. Chem.* **1982**, *54*, 1720.
(49) Parker, V. D.; Handoo, K. L.; Roness, F.; Tilset, M. *J. Am. Chem. Soc.* **1991**, *113*, 7493.
(50) Wayner, D. D. M.; Parker, V. D. *Acc. Chem. Res.* **1993**, *26*, 287.